Weibel-Instability-Mediated Collisionless Shocks in the Laboratory with Ultraintense Lasers

F. Fiuza,[1,*] R. A. Fonseca,[1,2] J. Tonge,[3] W. B. Mori,[3] and L. O. Silva[1,†]

[1]*GoLP/Instituto de Plasmas e Fusão Nuclear—Laboratório Associado, Instituto Superior Técnico, Lisboa, Portugal*
[2]*Instituto Universitário de Lisboa, Lisboa, Portugal*
[3]*Department of Physics and Astronomy, University of California, Los Angeles, California 90095, USA*

The formation of nonrelativistic collisionless shocks in the laboratory with ultrahigh intensity lasers is studied via *ab initio* multidimensional particle-in-cell simulations. The microphysics behind shock formation and dissipation and the detailed shock structure are analyzed, illustrating that the Weibel instability plays a crucial role in the generation of strong subequipartition magnetic fields that isotropize the incoming flow and lead to the formation of a collisionless shock, similar to what occurs in astrophysical scenarios. The possibility of generating such collisionless shocks in the laboratory opens the way to the direct study of the physics associated with astrophysical shocks.

Understanding how collisionless shocks are formed and propagate in unmagnetized plasmas is of great importance to the study of many astrophysical scenarios such as γ-ray burst (GRB) afterglows, active galactic nuclei, pulsar wind nebulae, and supernova remnants [1–3]. The synchrotron radiation collected in astronomical observations suggests that these structures can generate subequipartition magnetic fields and accelerate particles to very high energies [4]. How the magnetic fields are generated and what their structure is, which dissipation mechanism is dominant, which physical processes lead to shock formation, and how particles are accelerated remain open questions.

Electromagnetic turbulence associated with the Weibel, or current filamentation, instability [5] is believed to be the leading mechanism for shock formation in weakly magnetized plasmas [6]. This instability can generate small-scale magnetic fields in counterstreaming plasmas which can scatter particles and isotropize the flow. Previous numerical studies of idealized astrophysical collisionless shock scenarios have shown, using particle-in-cell (PIC) codes, that Weibel instability can lead to strong filamentation, magnetic field generation, and shock formation [7,8] and that nonthermal particles can be accelerated in this shock structure [9,10] and emit synchrotron radiation [11]. The validation of these numerical studies for astrophysical scenarios, where *in situ* observations are not possible, is limited, since the information available from these astrophysical objects comes only from their radiation emission, which occurs at significantly larger temporal and spatial scales.

Laboratory experiments can play a crucial role in validating theoretical and numerical models of astrophysical phenomena [12]. In the last years, a few experimental studies have been proposed and conducted for the generation of nonrelativistic electrostatic collisionless shocks in the laboratory with colliding laser-ablated plasmas [13]. However, in the case of Weibel-instability-mediated collisionless shocks, the conditions for shock generation in the laboratory are not yet fully understood and no experimental evidence has been observed to date.

In this Letter, we demonstrate the possibility to generate truly Weibel-instability-mediated collisionless shocks in the laboratory by the interaction of an ultraintense laser pulse with an overcritical plasma. Using *ab initio* multidimensional relativistic PIC simulations, we examine in detail the physics behind shock formation and propagation, from the generation of the incoming flow by the intense laser to the microinstabilities that lead to the generation of subequipartition magnetic fields that isotropize the flow and lead to the formation of the shock structure. We show that the underlying physics is similar between these nonrelativistic laser-driven shocks in the laboratory and previously considered relativistic astrophysical shocks, illustrating the possibility of directly studying the physical mechanisms behind these astrophysical scenarios in the laboratory.

In order to study the self-consistent shock formation and propagation in realistic laboratory conditions we use two-dimensional (2D) and three-dimensional (3D) simulations performed with the PIC code OSIRIS [14]. We simulate the interaction of an ultraintense laser pulse with a preionized unmagnetized electron-proton plasma. The laser is linearly polarized and has a wavelength of 1 μm. We have simulated different laser intensities, ranging from 10^{20} to 10^{22} W cm^{-2}, corresponding to a normalized laser vector potential $a_0 \sim$ 10–100, and different plasma densities, ranging from 10 to $100 n_c$, where n_c is the critical density for 1 μm light. The initial plasma temperature is 1 keV. The computational domain is typically $80 c/\omega_{\mathrm{pi}}$ in the longitudinal direction and $18 c/\omega_{\mathrm{pi}}$ in the transverse direction, with $c/\omega_{\mathrm{pi}} = c(4\pi Z^2 e^2 n_p/m_i)^{-1/2}$ the ion skin depth for a plasma density n_p and ion mass m_i; e is the elementary charge, Z is the charge state, and c the speed of light in vacuum. The system is numerically resolved with

2 cells per c/ω_{pe} in both directions and uses 64 particles per cell for each species, for a typical total of 10^9 particles. We note that these are the first full-scale simulations of unmagnetized electron-ion shocks (previous simulations used either positrons or ions with reduced mass ratios).

As the intense laser hits the overdense target it acts like a piston, pushing the front of the target as a massive and uniform flow but also generating a population of fast or hot electrons. Fast electrons, which typically have a density on the order of the critical density n_c and a relativistic factor $\gamma_0 \simeq \sqrt{1 + a_0^2}$ are not affected by the proton response and propagate through the target. A cold return current is set up in order to balance the incoming fast electron flux. The two counterstreaming flows go Weibel unstable, similar to what is believed to occur in astrophysics [6–11]. Even in the case where the laser-generated incoming flow is too hot to filament by itself in the background plasma, the return current is cold and therefore filaments. Following the usual procedure for the calculation of the dispersion relation for purely transverse modes [15], and in the limit of a hot and rarefied electron flow counterstreaming with a cold and dense slowly drifting electron background, the maximum electron Weibel-instability growth rate can be shown to be simply $\Gamma_{We} \simeq (\beta_r/\sqrt{\gamma_r})\omega_{pe}$, where β_r is the normalized velocity of the returning electrons and γ_r their Lorentz factor. In order to establish current neutrality, $\beta_r \simeq n_c/n_p$, yielding $\Gamma_{We} = 0.01$–$0.1\omega_{pe}$ for the parameters in study and leading to the generation of strong magnetic fields in a few $100\omega_{pe}^{-1}$. The electron instability saturates when the magnetic energy density in the Weibel filaments becomes comparable to the energy density in the fast electron flow, leading to a saturation magnetic field amplitude $B_{sat} \simeq (8\pi a_0 n_c m_e c^2)^{1/2}$, for ultrahigh laser intensities ($a_0 \gg 1$). The magnetic fields associated with Weibel or current filamentation instability of the fast electron flow isotropize the incoming nonrelativistic electron-proton flow, leading to a strong compression and to the formation of a shock, defined as the density compression that propagates away from the laser-plasma interface. The shock speed is determined by the slowdown and mass or pressure buildup associated with this more massive flow, and therefore it is nonrelativistic. Once the shock is formed, the particles that escape the shock from the downstream still provide the generation of the counterstreaming cold return current in the upstream, which allows for continuous filamentation in the upstream region.

For the collisionless shock to be formed in the unmagnetized plasma, it is required that the piston (downstream) velocity exceeds the ion sound speed, $c_S = (Zk_B T_e/m_i)^{1/2}$, where k_B is the Boltzmann constant, and T_e is the bulk electron temperature, which is typically a fraction $\alpha \sim \frac{1}{3}$–$\frac{1}{2}$ of the ponderomotive temperature before the shock is formed [16], $k_B T_e \simeq \alpha a_0 m_e c^2$. The downstream velocity, v_d, can be estimated by equating the momentum flux of the incoming mass flow with the laser-light pressure, yielding a normalized velocity of $\beta_d = v_d/c = \sqrt{(n_c/2n_p)(Zm_e/m_i)a_0^2}$ [17]. The condition for shock formation, $v_d > c_S$, is then given as a function of laser and plasma parameters by

$$a_0 \gtrsim 2\alpha \frac{n_p}{n_c}. \tag{1}$$

Figure 1 illustrates the main features of shock formation for a typical simulation where we have used a laser intensity of 5×10^{21} W cm^{-2} ($a_0 = 60$) and a plasma density of $50n_c$. A strong compression is observed in the downstream [Figs. 1(a) and 1(b)], between the laser-plasma interface and the shock front, and strong filamentation in the upstream region. The magnetic field illustrates similar
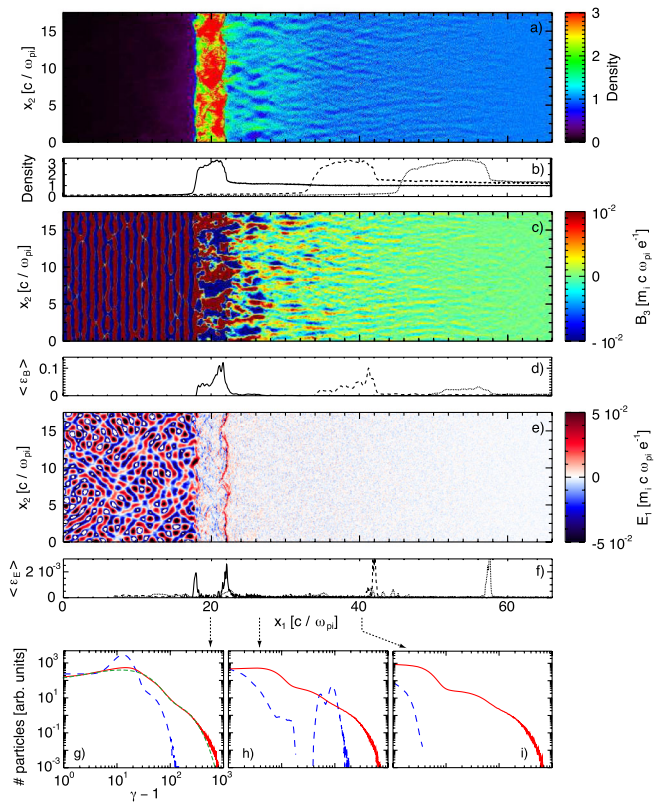

FIG. 1 (color online).   Steady-state structure of a collisionless shock generated through the irradiation of an overcritical unmagnetized plasma by an ultraintense laser pulse after 385 fs ($113\omega_{pi}^{-1}$) of interaction. (a) Density structure normalized to the unperturbed upstream density. (b) Transversely averaged plasma density. (c) Magnetic field in the direction outside the simulation plane. (d) Transversely averaged magnetic energy. (e) Longitudinal electric field. (f) Transversely averaged electric energy. (g)–(i) Electron and ion (scaled up by the mass ratio m_i/m_e) spectrum at three different slices (positions marked by arrows). Red solid lines, electrons; blue dashed lines, ions; green dotted lines, fit to a sum of two 2D Maxwellian distributions. The transversely averaged quantities in (b), (d), and (f) are also shown for interaction times of 805 fs ($250\omega_{pi}^{-1}$) (dashed lines) and 1134 fs ($353\omega_{pi}^{-1}$) (dotted lines).

filamentary structures [Fig. 1(c)]. The filament size evolves from the electron skin depth c/ω_{pe}, far upstream, to the ion skin depth c/ω_{pi}, close to the shock, and are then frozen behind the shock front. The shock transition is about $(1-2)c/\omega_{pi}$ thick, at early times, which is of the order of the ion Larmor radius, and corresponds to a peak in the magnetic energy [Fig. 1(d)]. At later times, the thickness of the magnetic energy peak continuously increases towards the downstream region, as observed in previous astrophysical configurations [18], reaching values of the order of $10c/\omega_{pi}$ for our largest interaction times, $500\omega_{pi}^{-1}$. The transversely averaged magnetic field energy density reaches 12% of equipartition with the upstream kinetic energy density (measured in the downstream rest frame), i.e., $\epsilon_B = (B^2/8\pi)/[n_p m_i c^2(\gamma_d-1)] \simeq 0.12$, for the measured $v_d \simeq 0.13c$ [Fig. 1(d)]. Locally, the magnetic field energy density at the shock front can reach equipartition with the upstream, $\epsilon_{B,max} \simeq 1$. These values are fully consistent with previous simulations of Weibel-instability-mediated relativistic shocks in astrophysical scenarios [7–10], indicating similar underlying physical mechanisms. An important difference is the well-defined longitudinal electric field observed at the shock front in our simulations [Fig. 1(e)]. This is associated with the fact that downstream electrons are significantly hotter than ions, since the laser predominantly heats electrons. This was not observed in previous simulations of relativistic counterstreaming plasmas, as both electron and ion flows are initialized completely cold, which will hardly be the case in a laser-driven laboratory configuration. Although the energy associated with this electric field is relatively small, $\epsilon_E = (E^2/8\pi)/[n_p m_i c^2(\gamma_d-1)] \simeq 0.025$ [Fig. 1(f)], the field is able to reflect a fraction of the upstream ion population (10–15%). As these reflected ions counterstream with the background plasma, they will lead to an enhancement of the magnetic fields in the ion time scales due to Weibel instability in the ions. In the limit of cold ions, the maximum ion Weibel-instability growth rate is given by $\Gamma_{Wi} \simeq \beta_b \sqrt{(n_b/n_p)/(\gamma_b m_i)}\,\omega_{pe} \simeq 2\beta_{sh}\sqrt{(n_b/n_p)/m_i}\,\omega_{pe}$, where n_b is the density of the reflected ion beam, which moves with twice the shock velocity. We can indeed see that in the foot of the shock (region where the reflected ions are present), the Weibel magnetic fields are stronger than in the remaining upstream region [Fig. 1(c)]. At this point the instability becomes similar to more conventional scenarios with two counterstreaming plasma flows, but where the electrons are relativistic and the ions are nonrelativistic. It should be noted that an electrostatic ion-ion instability associated with the reflected ions has been previously identified in electrostatic shocks, strongly affecting its structure [19]. It can be shown, following the usual procedure for the calculation of the dispersion relation for electrostatic modes [19], that in the limit of cold ion flows, the maximum growth rate of the ion-ion electrostatic instability is

$\Gamma_{Ei} \simeq \sqrt{(n_b/n_p)/(8m_i)}\,\omega_{pe}$. This instability tends to dominate over the Weibel instability in the case of low shock velocities ($\beta_{sh} < 0.1$); however, for the large shock velocities reached in our proposed setup ($\beta_{sh} > 0.1$) the Weibel instability dominates, further amplifying the magnetic fields and isotropizing the incoming flow. This has been confirmed by simulating the propagation of an ion flow in a plasma background for the densities and velocities associated with our setup, and for different ion temperatures (1 eV–1 keV) (not shown here). The condition $\beta_{sh} > 0.1$ effectively defines a lower limit for the laser intensity required to drive Weibel-instability-mediated shocks in this configuration.

The particle spectrum at different longitudinal positions is highly modified by the shock structure. In the downstream region [Fig. 1(g)], we observe a two-temperature electron spectrum from the laser acceleration, which can be reasonably fitted to a sum of 2D Maxwellian distributions of the form $f(\gamma) = a_1 \gamma \exp(-\gamma/\Delta\gamma_1) + a_2 \gamma \exp(-\gamma/\Delta\gamma_2)$, with normalizations a_1 and a_2, $\Delta\gamma_1 = 13$, and $\Delta\gamma_2 = 58$, which is close to the expected laser-induced ponderomotive temperature of $\Delta\gamma = \sqrt{1+a_0^2} \simeq 60$ [17]. The bulk electron temperature, $\Delta\gamma_1$, which initially is a fraction α of the ponderomotive temperature, changes as the shock is formed and most of the particles are trapped behind it, leading to an equipartition between the electron thermal energy and the ion fluid energy, i.e., $\Delta\gamma_1 = (\gamma_d-1)m_i/m_e$. The most energetic electron population crosses the shock front into the upstream and remains relatively unchanged as evidenced by the spectra at the foot of the shock [Fig. 1(h)] and in front of it [Fig. 1(i)]. The ions are heated up in the downstream [Fig. 1(g)]. As the filaments merge in the vicinity of the shock front and the magnetic fields of the filaments coalesce, the energy in the fields is converted back to thermal energy of the ions in the downstream region, thus leading to an effective heating of the ions and electrons. We observe that in the upstream region, the initial ion flow moving towards the shock loses 20–25% of its energy for electron heating, and another 20–25% goes into ion heating (thermal energy) in the downstream. These numbers are comparable, but lower than the observed values in idealized astrophysical configurations [20]. In the foot region, we observe the presence of a small ion population that has been reflected at the shock front [Fig. 1(h)].

The generated shock structure has a well-defined velocity and density jump. The shock hydrodynamic jump conditions [21] predict a density jump with a downstream to upstream density ratio $n_2/n_1 = (\Gamma_{ad}\gamma_d + 1)/(\Gamma_{ad} - 1)$ and normalized velocity of $\beta_{sh} \equiv v_{sh}/c = [(1 + \Gamma_{ad}\gamma_d) \times (\gamma_d^2 - 1)^{1/2}]/[1 + \gamma_d + \Gamma_{ad}(\gamma_d^2 - 1)]$, where Γ_{ad} is the adiabatic index and γ_d is the Lorentz factor of the downstream in the frame of the upstream (which for this case is the laboratory frame, since the upstream is approximately at rest). In the nonrelativistic limit, where $\beta_d \ll 1$ and
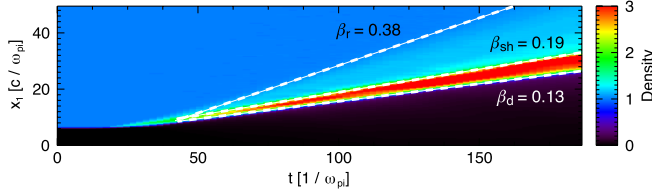
FIG. 2 (color online). Temporal evolution of the transversely averaged density profile illustrating the normalized velocity of the downstream β_d, the shock β_{sh}, and the ions that are reflected at the shock front β_r.

$\gamma_d \sim 1$, the density jump can be written as $n_2/n_1 = (\Gamma_{ad} + 1)/(\Gamma_{ad} - 1)$ and the shock velocity as

$$\beta_{sh} \simeq \frac{a_0}{2}\sqrt{\frac{n_c}{2n_p}\frac{Zm_e}{m_i}}(1 + \Gamma_{ad}), \qquad (2)$$

provided that the plasma is always opaque to the incoming light, i.e., that the downstream density is higher than the relativistic critical density $n_p(\Gamma_{ad} + 1)/(\Gamma_{ad} - 1) > n_c\sqrt{1 + a_0^2}$. For the case of Fig. 1, we observe a density jump of ~ 3.1 and a normalized shock velocity of ~ 0.19 [Fig. 2], which are in very good agreement with the derived theoretical values of 3 and 0.2, respectively, for an adiabatic index of 2, appropriate for a 2D gas.

In order to understand if our 2D simulations can capture the relevant 3D physics, we have performed 3D simulations for the same parameters of Fig. 1. A similar shock structure has been obtained with a normalized shock velocity of 0.18, which is consistent with Eq. (2) for an adiabatic index of 5/3, appropriate for a 3D gas. Previous PIC studies of shock formation in intense laser-plasma interactions have focused on the 1D dynamics [22] and, therefore, could not evaluate the role or impact of Weibel instability in these scenarios.

As evidenced by the shock jump conditions, the properties of Weibel-instability-mediated collisionless shocks generated in the laboratory in the configuration here proposed can be controlled by tuning the laser and plasma parameters. In particular, the shock velocity can be controlled by adjusting the laser intensity, I, the plasma density, n_p, and/or the target composition (ion mass, m_i, and charge state, Z) according to Eq. (2), affecting proportionally the energy of the ions reflected by the shock, $\epsilon_{ion}[MeV] \simeq 74.2ZI[10^{21}\,W\,cm^{-2}]/n_p[10^{22}\,cm^{-3}]$, which can be measured experimentally. This tunability is illustrated in Fig. 3, where we can see that the shock velocity obtained for different simulations with different laser and plasma parameters is in very good agreement with Eq. (2). Furthermore, the laser polarization can also be varied (from linear to circular) to control the laser electron heating and to study its influence in the shock properties.

The laser parameters required to study the generation of Weibel-instability-mediated collisionless shocks in the laboratory can be estimated based on our results. The laser
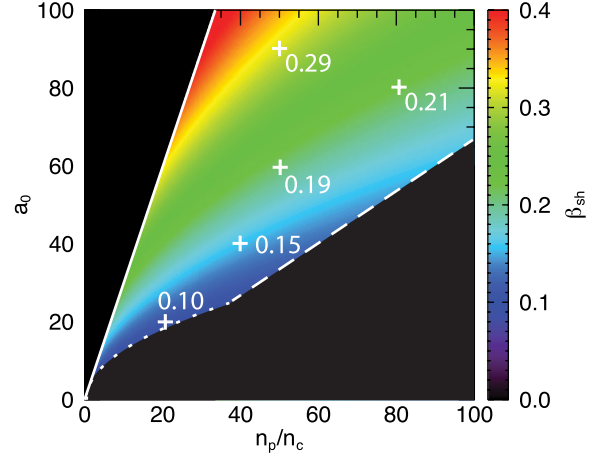

FIG. 3 (color online). Shock velocity as a function of the plasma density and the laser normalized vector potential. Numerical values on the plot indicate the shock velocity measured in simulations. The parameter range has an upper limit defined by the condition for relativistic opacity of the downstream plasma (solid) and lower limits defined by the condition for the Weibel instability to dominate over the electrostatic instability, $\beta_{sh} > 0.1$ (dotted), and by Eq. (1), with $\alpha = 1/3$ (dashed).

duration, τ_0, should be significantly longer than the shock formation time, t_f, which is on the order of the time it takes the piston to push the plasma a shock thickness forward, $t_f \simeq (\beta_d\omega_{pi})^{-1}$, i.e., $\tau_0 \gtrsim 10(\beta_d\omega_{pi})^{-1}$ or $\tau_0[ps] \gtrsim 0.5\frac{m_i}{m_p}[I_0[10^{21}\,W\,cm^{-2}]Z^3]^{-1/2}$, where m_p is the proton mass. The laser spot size should be much larger than the shock thickness in order to have a stable shock front, $W_0 \gtrsim 10c/\omega_{pi}$ or $W_0[\mu m] \gtrsim 10(\frac{m_i}{m_p})^{1/2}\frac{\lambda_0[\mu m]}{Z}(\frac{n_p}{50n_c})^{-1/2}$. By combination of the two previous conditions, the laser energy required to provide a stable shock structure is $\epsilon_0[kJ] \simeq 1.5(\frac{I_0[10^{21}\,W\,cm^{-2}]}{Z^7})^{1/2}(\frac{m_i}{m_p})^2(\lambda_0[\mu m])^2(\frac{n_p}{50n_c})^{-1}$, which is readily available with current picosecond kJ class lasers.

In conclusion, we have shown that in realistic laboratory conditions the plasma flow generated by the interaction of an ultraintense laser pulse with an overcritical target can lead to the generation of subequipartition magnetic fields, due to Weibel or current filamentation instability, that isotropize the flow and generate a shock. The shock structure and its properties, here shown for the first time for realistic ion to electron mass ratios, are similar to previously simulated low-mass-ratio Weibel-instability-mediated collisionless shocks in idealized astrophysical scenarios. Our results illustrate the possibility of studying for the first time in the laboratory the physics behind the formation and propagation of Weibel-instability-mediated collisionless shocks in unmagnetized plasmas, which would allow for a better understanding of the role of these structures in nonthermal particle acceleration and emission of synchrotron radiation in astrophysical scenarios.

*frederico.fiuza@ist.utl.pt

†luis.silva@ist.utl.pt

[1] R. Blandford and D. Eichler, Phys. Rep. **154**, 1 (1987).

[2] T. Piran, Rev. Mod. Phys. **76**, 1143 (2005).

[3] E. Waxman, Plasma Phys. Controlled Fusion **48**, B137 (2006).

[4] F. C. Jones and D. C. Ellison, Space Sci. Rev. **58**, 259 (1991).

[5] E. S. Weibel, Phys. Rev. Lett. **2**, 83 (1959).

[6] A. Gruzinov and E. Waxman, Astrophys. J. **511**, 852 (1999); M. V. Medvedev and A. Loeb, *ibid.* **526**, 697 (1999).

[7] L. O. Silva, R. A. Fonseca, J. W. Tonge, J. M. Dawson, W. B. Mori, and M. V. Medvedev, Astrophys. J. **596**, L121 (2003); K. I. Nishikawa, P. Hardee, G. Richardson, R. Preece, H. Sol, and G. J. Fishman, *ibid.* **595**, 555 (2003); J. T. Frederiksen, C. B. Hededal, T. Haugbolle, and A. Nordlund, *ibid.* **608**, L13 (2004); M. V. Medvedev, M. Fiore, R. A. Fonseca, L. O. Silva, and W. B. Mori, *ibid.* **618**, L75 (2005); T. N. Kato and H. Takabe, *ibid.* **681**, L93 (2008);

[8] A. Spitkovsky, Astrophys. J. **673**, L39 (2008).

[9] A. Spitkovsky, Astrophys. J. **682**, L5 (2008).

[10] S. F. Martins, R. A. Fonseca, L. O. Silva, and W. B. Mori, Astrophys. J. **695**, L189 (2009).

[11] L. Sironi and A. Spitkovsky, Astrophys. J. **707**, L92 (2009).

[12] B. Remington, D. Arnett, R. P. Drake, and H. Takabe, Science **284**, 1488 (1999); B. Remington, R. P. Drake, and D. D. Ryutov, Rev. Mod. Phys. **78**, 755 (2006).

[13] H. Takabe *et al.*, Plasma Phys. Controlled Fusion **50**, 124057 (2008); L. Romagnani *et al.*, Phys. Rev. Lett. **101**, 025004 (2008); Y. Kuramitsu *et al.*, Phys. Rev. Lett. **106**, 175002 (2011).

[14] R. A. Fonseca *et al.*, Lect. Notes Comput. Sci. **2331**, 342 (2002); R. A. Fonseca, S. F. Martins, L. O. Silva, J. W. Tonge, F. S. Tsung, and W. B. Mori, Plasma Phys. Controlled Fusion **50**, 124034 (2008).

[15] L. O. Silva, R. A. Fonseca, J. W. Tonge, W. B. Mori, and J. M. Dawson, Phys. Plasmas **9**, 2458 (2002); N. Shukla, A. Stockem, F. Fiuza, and L. O. Silva, J. Plasma Phys. **78**, 181 (2012).

[16] J. May, J. Tonge, F. Fiuza, R. A. Fonseca, L. O. Silva, C. Ren, W. B. Mori, Phys. Rev. E **84**, 025401(R) (2011).

[17] S. C. Wilks, W. L. Kruer, M. Tabak, and A. B. Langdon, Phys. Rev. Lett. **69**, 1383 (1992).

[18] U. Keshet, B. Katz, A. Spitkovsky, and E. Waxman, Astrophys. J. **693**, L127 (2009).

[19] T. N. Kato and H. Takabe, Phys. Plasmas **17**, 032114 (2010).

[20] In Ref. [8], the electrons gain 35% of the incident ion energy in the upstream, and most of the remaining ion energy goes into heating at the downstream.

[21] R. Blandford and C. F. McKee, Phys. Fluids **19**, 1130 (1976).

[22] J. Denavit, Phys. Rev. Lett. **69**, 3052 (1992); L. O. Silva, M. Marti, J. R. Davies, R. A. Fonseca, C. Ren, F. S. Tsung, and W. B. Mori, Phys. Rev. Lett. **92**, 015002 (2004).